Aggregation of Hybrid Farm in Grid Following and Grid Forming Modes for Short Circuit Studies

Shah Mohazzem Hossain, Trupal Patel, Sukumar Brahma
Holcombe Department of Electrical and Computer Engineering
Clemson University, SC, United States
Email: shossai, tpatel, sbrahma@clemson.edu

Matthew J. Reno
Sandia National Laboratories
Albuquerque, NM, United States
Email: mjreno@sandia.gov

***Abstract*—Hybrid renewable farms with a mix of solar and wind resources, along with a bulk energy storage system (BESS) are growing. Such farms include numerous inverters, pad-mounted transformers, collector feeders, and dc-side components depending on the type of generation. Additionally, inverters in such farms typically employ different control strategies, such as 'grid following' (GFL) and 'grid forming' (GFM), based on the resource type or system requirements, where an inverter exhibits similar steady-state response but different fault behavior. This paper lays out a physics-based hypothesis to advocate the use of an aggregated model, while avoiding detailed modeling of all components of a hybrid farm. The hypothesis is substantiated by simulation of a hybrid farm using Electromagnetic Transient (EMT) Program, documenting how hybrid farms should be aggregated for short circuit studies with minimal errors.**

***Index Terms*—BESS, fault, inverter, short circuit, solar farm, wind farm.**

I. Introduction

A hybrid farm comprises of solar, wind, and bulk BESS system (BESS) operating in a single farm. Over the past few years, there has been a rapid growth in installation of hybrid farms in the United States (US). According to a recent report by Berkeley Lab [1], five such hybrid farms are currently operational, and additional 28 farms with a total capacity of 12 GW are in the pipeline, and one under construction in Oklahoma [2].

As modeling of inverters, even if averaged, is computationally expensive. Aggregated model that can reduce the farm to a single equivalent inverter is therefore highly desirable. We have shown in [3] that such aggregation is possible for solar and Type-IV wind farms that deploy 'grid following' (GFL) controls. This was possible because the combined impedance of the pad-mounted transformer and the inverter-filter reflected to the collector side is much greater than that of the collector cables. The GFL control used in [3] acts as a power-regulated current source for the grid [4]. It uses grid voltage and frequency as references, synchronizes with the grid voltage angle, and adjusts its internal voltage magnitude to produce the necessary real and reactive power output. However, its inability to independently regulate voltage and frequency has raised concerns about system stability, especially for a large penetration [5]. To address these concerns, another type of control known as 'grid forming' (GFM) has emerged. In this mode, inverter behaves as a controllable voltage source and adjusts its internal voltage magnitude and angle to synchronize with the grid voltage and frequency [6]. It effectively regulates active and reactive power to provide essential support to the grid by adjusting the angle of internal voltage and closely mirrors the functionality of a synchronous generator, thus ensuring system stability. Hence, while grid-connected, the steady-state performance of these two controls is almost the same and follows the unit commitment commands, but their fault behavior significantly differs.

As the next step in our studies on aggregating EMT models of inverter based resources (IBRs), this paper presents a study of aggregation of hybrid farms with inverters employing GFL, GFM or both modes of control. It first explains these control modes and how they are modeled. Then, it simulates a scaled 26 MW hybrid farm in Simulink to illustrate how it can be aggregated for short-circuit studies in EMT simulations. It also explores the impact of increasing line lengths in the collector network on the proposed aggregation.

II. Modeling Inverter Control Modes

An inverter with a 2 MVA, 690V rating is modeled, to be used for both, solar and Type IV WTG units, in either GFL or GFM mode, based on a switch position as seen in its control diagram in Fig. 1, which also includes a droop control unit, low voltage ride-through (LVRT) unit, and both current and voltage control units. The droop control unit, modeled based on [6], demonstrates a linear trade-off between frequency and voltage, enabling voltage regulation and automatic load sharing among multiple inverters.

In GFL mode, its control is designed in conventional dq reference frame, as described in [7]. This design incorporates Siemens Gamesa logic from [8] to generate current references when the inverter terminal voltage $(V_t^{(1)})$ falls below 0.9 per unit (pu), entering into LVRT operation. It supplies only positive sequence current output, even during unsymmetrical fault scenarios.

This material is based upon work supported by the U.S. Department of Energy's Office of Energy Efficiency and Renewable Energy (EERE) under the Wind Energy Technologies Office (WETO) through Sandia National Laboratories is a multimission laboratory managed and operated by National Technology and Engineering Solutions of Sandia, LLC, a wholly owned subsidiary of Honeywell International Inc., for the U.S. Department of Energy's National Nuclear Security Administration under contract DE-NA0003525.

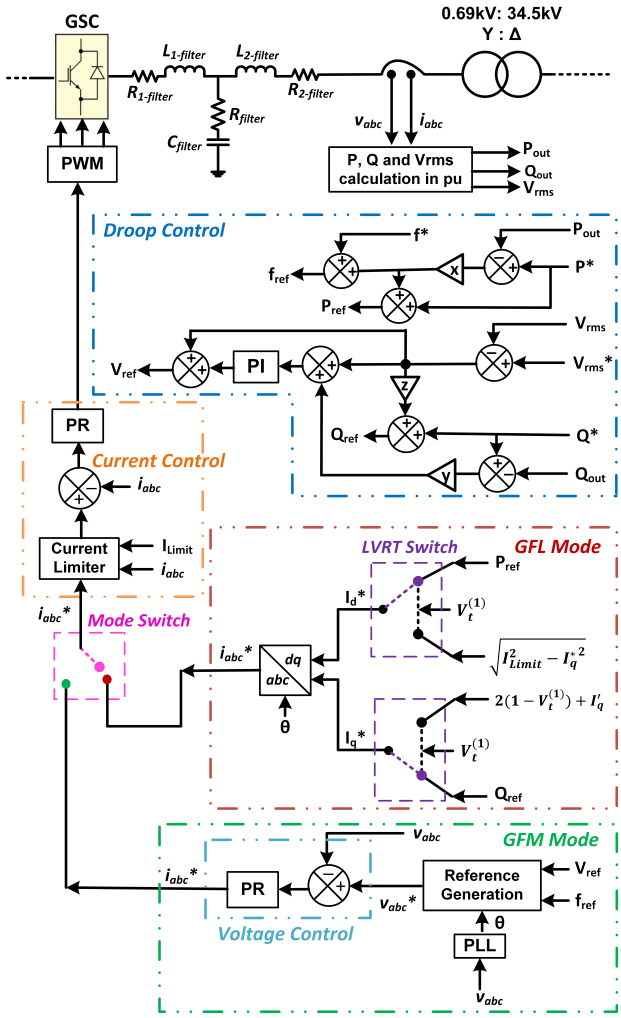

Fig. 1. Control diagram of the inverter model.

In GFM control, described in [9], droop-derived voltage magnitude ($\mathrm{V_{ref}}$) and frequency ($\mathrm{f_{ref}}$) reference values create a pre-requisite instantaneous voltage reference. This reference is then fed into a voltage control loop to generate the necessary current references. This control loop uses proportional-resonant (PR) control in the natural (abc) reference frame due to its superior performance over proportional-integral (PI) control [9]. The generated current reference includes both positive and negative sequence components, resulting in both positive and negative sequence current outputs during GFM operation, especially evident during unsymmetrical faults.

The current reference generated from either GFL or GFM mode of operation is fed into a common current control loop that uses current reference in the abc reference frame. Therefore, current references generated in the dq reference frame in GFL mode are converted to the abc reference frame before being fed into the current control loop. In this loop, the reference current passes through a current limiter block, designed based on [9], to ensure current output within inverter's maximum current limit of 1.3 pu based on [8] to model inverter overcurrent protection. Subsequently, the generated reference undergoes a comparison with the output current, and finally, the result is fed into a PR controller to generate the modulation waveform required for the pulse width modulation (PWM) control.

III. Modeling of Hybrid Farm

Fig. 2 shows the topology of the scaled 26 MW hybrid farm, implemented in MATLAB (Simulink) and consisting of five units each of 2 MW solar and wind generation, and a 6 MW, 24 MWh BESS unit. Since only the fundamental fault response is needed, an averaged inverter model is chosen [10] to reduce the computation burden. Justification for the choice of cable lengths can be found in [3]. The farm is operated at unity power factor to deliver maximum real power to the grid under normal operation. Description of components of the IBRs in the farm follows.

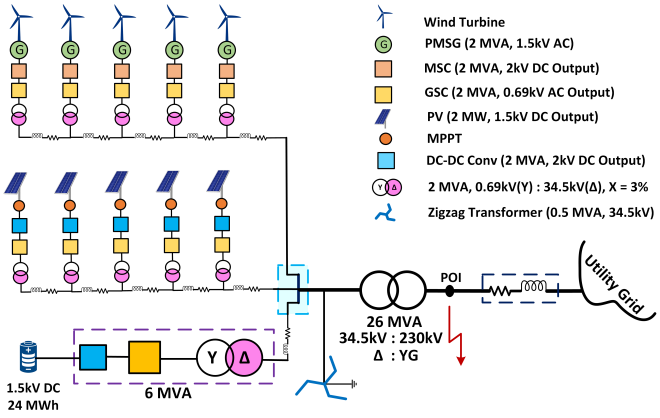

Fig. 2. Scaled hybrid farm model.

A. Solar Farm

1) Photovoltaic (PV) Array: This hybrid farm consists of five PV arrays, each rated at 1.5 kV (dc), 2 MW. In this model, constant values for irradiance and temperature are applied to achieve the maximum real power output during simulation. These are kept constant during faults, which last only for a few fundamental cycles. The generated voltage and current from each PV array are then fed into a maximum power point tracker (MPPT) unit, which extract the maximum energy from an array at the time of operation.

2) dc-dc Converter: The dc output voltage generated by each PV array is regulated through an individual dc-dc boost converter to maintain a constant input voltage to the inverter dc-terminal for any variation in input voltage (not an issue here due to constant temperature and irradiance), which is then boosted to 2 kV dc-output at the inverter terminal through a dc-link capacitor.

3) Grid-Side Converter (GSC) Unit: Each GSC unit converts 2 kV dc to 690 V, 60 Hz ac. It employs the control strategy described in Section II and is capable of operating in either GFL or GFM mode. The LCL filter in Fig. 2 filters the harmonics and comprises of resistors (10 mΩ, 1 mΩ and 60 mΩ), inductors (370 μH and 105 μH), and a capacitor (600 μF).

B. Wind Farm

1) Wind Turbine Unit: This paper implements a generic GE 2 MW wind turbine model, designed according to [11], and is operated at a constant wind speed to ensure maximum energy extraction throughout the simulation and assumed that this value will not change significantly during a fault event that lasts only for a few fundamental cycles. This energy is then transferred to a Permanent Magnet Synchronous Generator (PMSG) unit which incorporates machine parameters from [11]. This unit converts the extracted mechanical energy into electrical energy at 1.5 kV ac output voltage, depending upon the constant wind speed.

2) Machine Side Converter (MSC) Unit: This unit has a diode-bridge rectifier that converts the ac output of the PMSG to a fixed 2 kV dc-voltage. Its control, based on [11], is set to the active power reference command, depending upon the mechanical power available in the wind, which will be converted to electrical power by the PMSG. It is connected to the GSC unit through a dc-link capacitor along with a dc-chopper circuit.

3) GSC Unit: This unit converts 2 kV dc to 690 V, 60 Hz ac. The same GSC as described in Section II is employed for the Type IV WTG as well.

C. Bulk Energy Storage System

The BESS is included to enhance the dispatchability of solar and wind resources [12]. It consists of a battery bank, a bi-directional dc-dc converter (buck-boost), and a GSC.

1) Battery Unit: This battery bank incorporating commercial Li-ion cells for their extended life cycle is modeled based on [13] to produce a nominal voltage of 1.5 kV and a nominal capacity of $4kA \times 4hours = 16kAh$ (6 MVA, 24 MWh).

2) Converter Unit and GSC: A buck-boost converter designed based on [13], is used to charge the battery cells at a 1.5 kV bucked dc-output voltage and discharge them at a 2 kV boosted dc-output voltage. Its 2 kV dc-output voltage serves as the input to the GSC unit, which employs the control strategy explained in Section II and provides a 690 V, 60 Hz ac output. Since the GSC, including its filter, is designed in pu, its parameters and the parameters of the pad mounted transformer are simply scaled up to increase the power rating to 6 MVA. In this model, BESS operates in discharging mode with a 90% state of charge of the battery bank to ensure the maximum current contribution from this unit during short circuit study.

IV. Aggregation of Hybrid Farm

In this model, the combined impedance of the LCL filter $(0.19\angle 86.7°\Omega)$ and the pad-mounted transformer $(7.14\angle 90°m\Omega)$ for an individual generation unit, when reflected to the collector side, is $492.82\angle 86.82°\Omega$. On the other hand, the impedance of the longest collector feeder is $0.373\angle 76.4°\Omega$, and the maximum collector impedance from the POI to any GSC unit is $1.46\angle 76.4°\Omega$. Given that the combined impedance of the inverter and transformer is overwhelmingly larger than the collector line impedances, the collector network can simply be ignored without significant error. Therefore, this paper, based on [3], ignores the collector network and considers the total of 11 inverters of this farm to be in parallel for the short circuit study. Additionally, since individual GSCs primarily control the fault current, all these inverters, along with the pad-mounted transformers, are lumped into a farm-equivalent single GSC and pad-mounted transformer [3]. While the dc-side components of all units may be affected by such an event, its impact on the system output and fault current is expected to be negligible during a fault time-frame of a few fundamental cycles. The following section further investigates this aggregation-hypothesis for different control modes.

A. GFL Mode

In this mode, all the 11 GSC units within the hybrid farm of Fig. 2 are operated in GFL mode. Following our hypothesis, this hybrid farm is aggregated into a farm-equivalent single inverter and pad-mounted transformer, ignoring the collector network, as shown in Fig. 3(a). The pad-mounted transformer is scaled to a rating of 26 MVA, and LCL filter components scaled to resistors (76 mΩ, 76 $\mu\Omega$, and 5 mΩ), inductors (28.46 μH and 8.1 μH), and capacitor (7800 μF) [3]. Then, to compare the fault current output of the lumped hybrid farm model with the detailed model, a single line to ground (SLG), line to line (LL), and 3ϕ fault with a fault resistance of $1m\Omega$, are created at the POI terminal of both models at 3s, which are cleared at 3.2s. The instantaneous voltage and current outputs

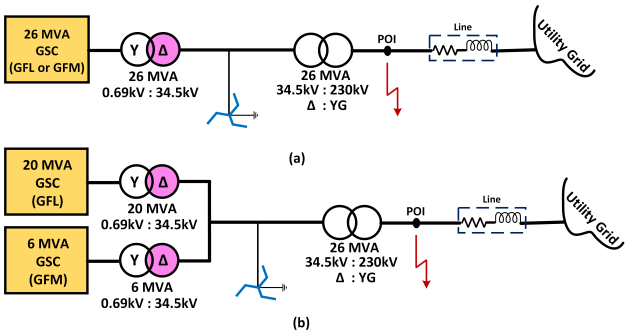

Fig. 3. Hybrid farm model aggregated as (a) GFL or GFM, (b) GFL and GFM.

at the POI of both models during a LL (BC) fault event are shown in Fig. 4, where 'det' and 'agg' represent responses of the detailed model and aggregated model, respectively. Since all GSCs operate in GFL mode with a current limit of 1.3 pu, only balanced positive sequence currents are injected by the GSCs during all the faults, as observed in the instantaneous current output of Fig. 4(b). The responses from both models essentially overlap, indicating minimal error. For a more comprehensive analysis, the phasor values of the measured voltage and currents were calculated using a moving window DFT. Errors in phasor values obtained for all three types of faults are tabulated in Table I, which reveal that the maximum errors in voltage magnitudes and angles are less than 1%, and 1.5°, respectively. For currents the errors are less than 2% in

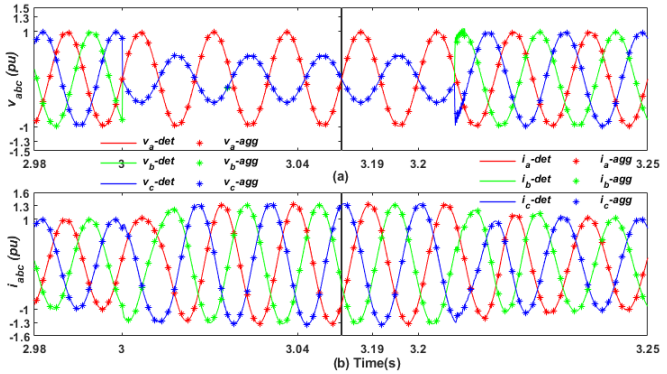

Fig. 4. GFL mode: Comparison of instantaneous outputs at POI during a BC fault - (a) terminal voltage, (b) injected current.

magnitude and 2° in angles. This validates the aggregation hypothesis for GFL mode of operation.

TABLE I
ERRORS IN PHASORS IN GFL MODE

Fault Type	Error (%∠°)	Cycle after Fault Inception				
		1st	2nd	3rd	4th	5th
SLG	$\|V\angle\theta\|$	0.32∠1.05°	0.27∠1.34°	0.19∠0.33°	0.18∠0.24°	0.14∠0.14°
	$\|I\angle\theta\|$	0.77∠0.48°	1.37∠0.27°	1.82∠0.25°	1.42∠0.22°	1.22∠0.21°
LL	$\|V\angle\theta\|$	0.18∠0.34°	0.22∠0.24°	0.24∠0.25°	0.21∠0.21°	0.32∠0.37°
	$\|I\angle\theta\|$	1.39∠0.87°	1.99∠1.42°	1.08∠1.41°	0.45∠0.77°	0.48∠0.71°
3ϕ	$\|V\angle\theta\|$	0.21∠0.68°	0.20∠0.67°	0.15∠0.05°	0.17∠0.03°	0.13∠0.02°
	$\|I\angle\theta\|$	0.45∠0.68°	0.65∠0.88°	0.31∠0.84°	0.14∠0.61°	0.16∠0.59°

B. GFM Mode

In this mode, all the 11 GSC units within the hybrid farm of Fig. 2 are operated in GFM mode. For this simulation, the same aggregated model is used (Fig. 3(a)), but the control mode is switched to GFM. The same fault scenarios were simulated, as mentioned in Section IV-A. The instantaneous voltage and current outputs at the POI of both models during a LL (BC) fault event are illustrated in Fig. 5. Note that the fault current output significantly differs from that for GFL mode (Fig. 4(b)), because both positive and negative sequence currents are contributed in the GFM mode. Still, responses from both models essentially overlap in this case as well. The errors in phasor values for all three faults are tabulated in Table II, revealing that the maximum errors in voltage magnitudes and angles were less than 1% and 1°, respectively.

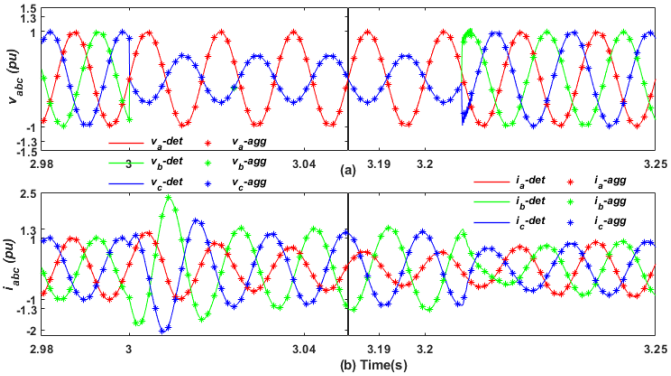

Fig. 5. GFM mode: Comparison of instantaneous outpus at POI during a BC fault - (a) terminal voltage, (b) injected current.

For currents, errors are less than 2% in magnitude and 1.5° in angles. This validates the aggregation hypothesis for GFM mode of operation as well.

TABLE II
ERRORS IN PHASORS IN GFM MODE

Fault Type	Error (%∠°)	Cycle after Fault Inception				
		1st	2nd	3rd	4th	5th
SLG	$\|V\angle\theta\|$	0.33∠1.45°	0.49∠1.54°	0.29∠0.31°	0.21∠0.34°	0.26∠0.38°
	$\|I\angle\theta\|$	0.87∠0.52°	0.83∠0.08°	0.93∠0.15°	0.71∠0.12°	0.80∠0.17°
LL	$\|V\angle\theta\|$	0.23∠0.56°	0.19∠0.43°	0.31∠0.35°	0.36∠0.34°	0.27∠0.28°
	$\|I\angle\theta\|$	1.87∠0.88°	1.76∠1.39°	1.13∠0.98°	0.63∠0.61°	0.68∠0.52°
3ϕ	$\|V\angle\theta\|$	0.24∠0.49°	0.17∠0.93°	0.13∠0.66°	0.22∠0.43°	0.15∠0.41°
	$\|I\angle\theta\|$	2.10∠0.87°	1.97∠0.92°	1.59∠0.89°	0.52∠0.37°	0.56∠0.32°

C. Mixed Modes

In this case, the solar and wind GSC units operate in GFL mode, while the GSC unit of the BESS operates in GFM mode, which is conventional in a hybrid farm configuration. In this case, this paper uses two lumped GSC units based on the mode of operation, as depicted in Fig. 3(b), instead of using a single inverter for the entire farm. This choice is made due to the different current outputs of GSCs in GFL and GFM operation during a fault event, as observed in Section IV-B. These two lumped GSC units filter and pad-mounted transformers are scaled by changing their corresponding base. Same fault scenarios were simulated, as created for the GFL and GFM modes. The instantaneous voltage and current outputs at the POI of both models during a LL (BC) fault event are shown in Fig. 6. Note that its fault current output differs

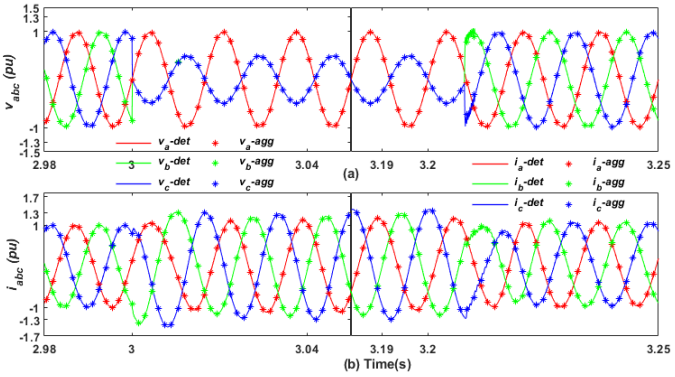

Fig. 6. Mixed mode with separate aggregation: Comparison of instantaneous outputs at POI during a BC fault - (a) terminal voltage, (b) injected current.

from the previous two cases, as it is the summation of both GFL and GFM operation current outputs. Still, the responses from both models overlap. The errors in phasor values for all three faults are tabulated in Table III, revealing that the maximum errors in voltage magnitudes and angles are less than 1% and 1°, respectively. For current, errors are less than 1.7% in magnitude and 1.5° in angles, which validates the aggregation hypothesis in mixed mode of operation with separate aggregation for GFL and GFM modes. However, if this mixed-mode operated hybrid farm is aggregated as a *single* GSC operated in either GFL or GFM, as done in section IV-A and IV-B, it leads to significantly higher errors in currents, as

TABLE III
ERRORS IN PHASORS IN MIXED MODE - SEPARATE AGGREGATION

Fault Type	Error (%∠°)	Cycle after Fault Inception				
		1st	2nd	3rd	4th	5th
SLG	$\lvert V\angle\theta\rvert$	0.13∠0.12°	0.19∠0.18°	0.15∠0.25°	0.23∠0.19°	0.14∠0.21°
	$\lvert I\angle\theta\rvert$	0.85∠0.52°	1.54∠0.28°	1.68∠0.25°	1.44∠0.23°	1.38∠0.26°
LL	$\lvert V\angle\theta\rvert$	0.13∠0.16°	0.29∠0.13°	0.24∠0.15°	0.26∠0.14°	0.17∠0.18°
	$\lvert I\angle\theta\rvert$	1.14∠1.20°	0.95∠0.64°	0.97∠0.70°	0.52∠0.63°	0.44∠0.57°
3ϕ	$\lvert V\angle\theta\rvert$	0.14∠0.09°	0.19∠0.13°	0.13∠0.16°	0.20∠0.12°	0.12∠0.11°
	$\lvert I\angle\theta\rvert$	1.09∠0.79°	0.73∠0.86°	0.42∠0.64°	0.31∠0.60°	0.36∠0.58°

listed in Table IV. This is obvious, since the output currents for GFL and GFM modes are significantly different as described in Sections IV-A and IV-B.

TABLE IV
ERRORS IN PHASORS IN MIXED MODE - SINGLE AGGREGATION

Fault Type	Error (%∠°)	Cycle after fault inception (GFL or GFM)					
		1st: GFL	2nd: GFL	3rd: GFL	1st: GFM	2nd: GFM	3rd: GFM
SLG	$\lvert V\angle\theta\rvert$	0.14∠0.28°	0.17∠0.21°	0.21∠0.13°	0.12∠0.30°	0.23∠0.28°	0.25∠0.14°
	$\lvert I\angle\theta\rvert$	6.91∠1.87°	18.24∠3.20°	17.20∠2.44°	21.41∠5.63°	60.16∠9.86°	61.77∠8.22°
LL	$\lvert V\angle\theta\rvert$	0.13∠0.18°	0.15∠0.12°	0.11∠0.15°	0.08∠0.17°	0.16∠0.16°	0.12∠0.11°
	$\lvert I\angle\theta\rvert$	17.64∠11.97°	20.35∠16.84°	20.65∠14.11°	68.79∠25.40°	76.57∠51.11°	41.84∠50.20°
3ϕ	$\lvert V\angle\theta\rvert$	0.09∠0.16°	0.11∠0.13°	0.14∠0.11°	0.12∠0.10°	0.13∠0.11°	0.14∠1.20°
	$\lvert I\angle\theta\rvert$	18.52∠8.62°	16.62∠13.97°	10.55∠11.68°	62.56∠13.59°	69.43∠41.79°	15.06∠41.22°

V. IMPACT OF COLLECTOR LENGTH ON AGGREGATION

As per Google Earth's measurements data of a real-world hybrid farm, this model adopts a minimum collector cable length of 0.40 km between two adjacent wind turbine units, which is more than three times the rotor diameter of a typical 2 MW wind turbine model. For solar units, this length is 0.27 km. To investigate the impact of the collector length on aggregation errors, we multiplied this original collector feeder lengths by a factor ranging from 2 to 12. Simulations were run for 1) GFL, 2) GFM, and 3) mixed mode with separate aggregations. The maximum errors observed in the voltage and current for each multiplier is shown in Fig. 7, where '*' indicates the actual error and '−−−' represents the corresponding error trend for each mode of operation. Errors in currents remain below 5% when the feeder lengths (hence impedance) are increased to 4 times the original feeder lengths, where the farthest inverter is situated more than 12 km away from the POI. This analysis suggests that the proposed aggregated models for all three types of operation provide acceptable accuracy for short-circuit studies in such types of hybrid farms.

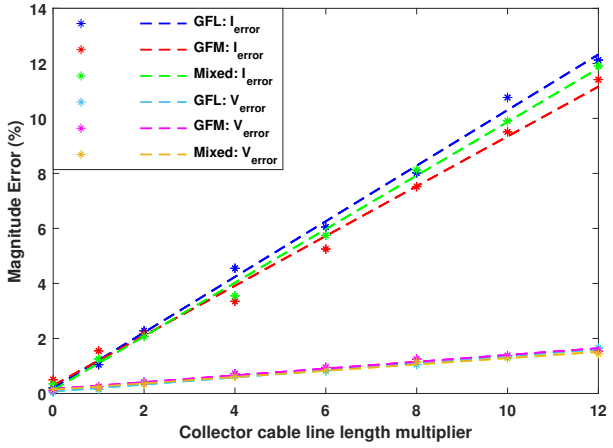

Fig. 7. Voltage and current errors with increasing length of collector cables.

VI. CONCLUSION

This paper illustrates that a hybrid farm, comprising of solar, wind, and BESS, can be aggregated by configuring all inverters in either GFL or GFM mode and lumping them into a single inverter of the same mode. This approach results in an error of less than 2% in current magnitude, which is acceptable for short circuit analysis. However, when a hybrid farm operating in both GFL (wind & solar) and GFM (BESS) modes is lumped into a single inverter that is operated only in either GFL or GFM mode, significantly larger errors are observed. Therefore, this type of aggregation should be avoided, and inverters operated in different modes should be aggregated separately. Additionally, a sensitivity analysis is performed to observe the impact of increasing collector feeder lengths, showing that the errors in fault currents increase with longer feeder lengths, but remain within 5% for cable lengths four times the lengths observed in real-world farms.

REFERENCES

[1] M. Bolinger, W. Gorman, J. Rand, and S. Jeong, "Hybrid power plants: status of operating and proposed plants," 2023.

[2] R. Walton, "Nextera inks 700 MW wind + solar + battery project, largest in the US," *Utility Dive*, July 29, 2019. [Online]. Available: https://www.utilitydive.com/news/nextera-inks-700-mw-wind-solar-battery-project-largest-in-the-us/559693/

[3] T. Patel, S. Brahma, and M. J. Reno, "Aggregation of solar and type 4 wind farms for short circuit studies," in *2023 IEEE Power & Energy Society Innovative Smart Grid Technologies Conference (ISGT)*. IEEE, 2023, pp. 1–5.

[4] Y. Lin, J. H. Eto, B. B. Johnson, J. D. Flicker, R. H. Lasseter, H. N. Villegas Pico, G.-S. Seo, B. J. Pierre, and A. Ellis, "Research roadmap on grid-forming inverters," National Renewable Energy Lab.(NREL), Golden, CO (United States), Tech. Rep., 2020.

[5] R. Rosso, X. Wang, M. Liserre, X. Lu, and S. Engelken, "Grid-forming converters: Control approaches, grid-synchronization, and future trends—a review," *IEEE Open Journal of Industry Applications*, vol. 2, pp. 93–109, 2021.

[6] W. Du, Y. Liu, F. K. Tuffner, R. Huang, and Z. Huang, "Model specification of droop-controlled, grid-forming inverters (GFMDRP_A)," Pacific Northwest National Lab.(PNNL), Richland, WA (United States), Tech. Rep., 2021.

[7] D. R. Kunwar and S. Brahma, "Analysis of the impacts of inverter based resources on the impedance matrix of power system," in *2023 IEEE Power Energy Society Innovative Smart Grid Technologies Conference (ISGT)*, 2023, pp. 1–5.

[8] "Modification of commercial fault calculation programs for wind turbine generators," *IEEE PES PSRC Report-TR78*, June 2020.

[9] T. Patel, P. Gadde, S. Brahma, J. Hernandez-Alvidrez, and M. J. Reno, "Real-time microgrid test bed for protection and resiliency studies," in *2020 52nd North American Power Symposium (NAPS)*, 2021, pp. 1–6.

[10] P. Gadde and S. M. Brahma, "Topology-agnostic, scalable, self-healing, and cost-aware protection of microgrids," *IEEE Transactions on Power Delivery*, vol. 37, no. 4, pp. 3391–3400, 2022.

[11] M. Singh and S. Santoso, "Dynamic models for wind turbines and wind power plants," National Renewable Energy Lab.(NREL), Golden, CO (United States), Tech. Rep., 2011.

[12] A. E. Momesso, P. H. Barra, P. I. Barbalho, E. N. Asada, D. V. Coury, J. C. Vieira, M. Oleskovicz, and M. Biczkowski, "Impact analysis of a transportable BESS on the short-circuit behavior in a distribution system," in *2020 IEEE Power & Energy Society General Meeting (PESGM)*. IEEE, 2020, pp. 1–5.

[13] M. Berger, I. Kocar, E. Farantatos, and A. Haddadi, "Modeling of Li-ion battery energy storage systems (BESSs) for grid fault analysis," *Electric Power Systems Research*, vol. 196, p. 107160, 2021.